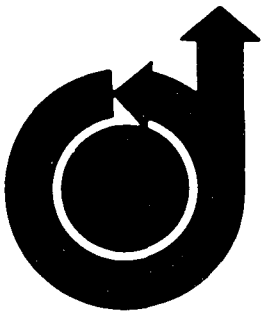

AIAA PAPER
75-226

SOME EXPERIMENTAL RESULTS ON THE L-STAR INSTABILITY OF METALLIZED COMPOSITE PROPELLANTS

by
R. N. KUMAR
California Institute of Technology
Pasadena, California

AIAA 13th Aerospace Sciences Meeting

PASADENA, CALIF. / JANUARY 20-22, 1975

SOME EXPERIMENTAL RESULTS ON THE L-STAR INSTABILITY OF METALLIZED COMPOSITE PROPELLANTS

R. N. Kumar
Daniel and Florence Guggenheim Jet Propulsion Center
California Institute of Technology, Pasadena, California

Abstract

Experimental results are reported on the L-star instability characteristics of three AP/composite propellants. The metal content of the propellants is 2%, 16%, and 16%. Chuffing, bulk mode oscillations, and time-independent combustion are observed with all three of these propellants. The stability boundary, defined as the boundary between time-independent and unstable combustion, is found to be well defined for two of the propellants in agreement with recognized trends available in the literature on other propellants. The frequency of bulk mode oscillations is presented as a function of the chamber characteristic length. One of the propellants tested has shown bulk mode instability at as high a pressure as 217 psia. All of these tests were performed in a stainless steel L^* motor with convenient, interchangeable stainless steel nozzles. The troublesome blockage of the small metal nozzles by the aluminum oxide slag was overcome in most of these tests by the application of viscous silicone oil on the nozzle surface before each run. This technique is being pursued further, with plans for the inclusion of silicone compounds in propellant formulation, to reduce heat transfer to the inert nozzle.

I. Introduction

Instability in solid propellant rocket motors continues to be a major problem in most, if not all, developmental programs. While sufficient understanding is not available at the present time to forestall (or even forecast) its occurrence, it is recognized that the contribution of the propellant itself to the instability is of crucial importance. For instance, it is known that "minor" compositional variations in propellant formulation can often make all the difference between stable and unstable operation in a motor. Extensive research is currently in progress to improve our understanding of instability. Of these, the more fundamentally oriented studies tend to select the simplest of situations for a detailed analysis. The L^* mode of combustion instability appears to be, by far, the simplest of unstable operations. On account of this simplicity, and its intrinsic interest, L^* instability has been the subject of extensive theoretical and experimental effort, as is evident from the list of references and related literature. Even for all of these efforts, some of which[10,16,21] are explicitly aimed at theoretically reconciling the experimental observations, the main conclusion at the present time appears to be (see, for example, ref. 14) that a fundamental understanding does not exist of this "simplest" form of instability.

The term L^* instability is used to denote any of several possible phenomena: chuffing, or intermittent combustion, bulk mode instability (BMI) involving periodic oscillations superposed on a mean chamber pressure, neither of which may have a constant value as time varies, and several combinations of these including the depressurization rate (dp/dt) extinguishment. The essential features of L^* instability were discussed by Price[2]. Additional experimental observations of the stability boundary (i.e., the boundary between time-independent and unstable combustion in the L^* mode), on frequency of oscillations and related quantities have been reported on various propellants[8-19]. Related work has appeared from many other centers also. In their studies on composite modified double-base propellants, Watermeier, et al.[1] found that the periodic agglomeration and shedding of aluminum led to low frequency instability. They also induced oscillations externally by having a siren over the exhaust. In general, there appears to be agreement[6-8,15] that aluminum tends to promote the low frequency instability because of this natural shedding frequency and also because the aluminum oxide is not effective at low frequencies in damping instability in the gas phase.

Considering the simpler system of non-metallized composite propellants, the frequency of BMI oscillations has shown good correlation with the chamber characteristic length (see ref. 11, for example). Standard normalizations of the frequency ($\omega\kappa/\bar{r}^2$) and the characteristic length ($L^* \div [(c^*\bar{r}^2)/(4\kappa RT_f)]$) have been found to correlate data rather well for some propellants[8,10]. It has been recognized for some time that the usual treatments that model the condensed phase as homogeneous may not be adequate to describe L^* instability and that the condensed phase heterogeneity may be the essence of BMI. Such "preferred frequency" oscillations were discussed in ref. 5 and given extensive coverage with bimodal oxidizer particles in ref. 14 where the natural length scale in the condensed phase was thought to be the oxidizer particle size. This "layered frequency" concept ($f = r/a$) indicates that a monomodal distribution of oxidizer particles in the propellant may lead to better defined results. Such monomodal distributions of AP particles in the same binder system (PBAN) were indeed used and extensive data were obtained[18,19]. The results showed[18] that the correlation of frequency with L^* was limited to each oxidizer particle size only and not universally valid when widely different monomodal oxidizer sizes were involved. The data processing indicated that the oxidizer particle size directly controls the frequency of oscillations, thus confirming the earlier layered-frequency concept.

Among the advantages of working with monomodal oxidizer particles is the important fact that the particle size which seems to be so important in L^* instability is much better defined than with multimodal distributions. However, it is recognized that even the monomodal distributions are not free from ambiguity in the existance of a distribution rather than a sharply defined size and the non-spherical shape of the particles. Nevertheless, these uncertainties are certainly less than what multimodal distributions offer.

Generalizing the same logic, it was planned to make the simplest of changes in these simple formulations to study the effect of metal on L^* instability. With the available data on the non-metallized version of the propellants, the tests were thought to

be the next logical step towards a better understanding of L* instability. Thus, the propellant that had shown extensive L* instability earlier[18,19] was chosen (Ã-13) and two per cent aluminum was included in place of AP. The data are presented both in the conventional way and in terms of the normalized variables developed in ref. 18.

In addition to this propellant, data have also been obtained on two other representative propellants from technological applications. One of them, LS-60, uses PBAN binder and a bimodal AP with 16% aluminum, and is thought to have its composition close to large booster candidates. The other propellant is the TPH. This uses the CTPB binder in a trimodal AP blend with 16% aluminum used in a bimodal blend. This propellant was used in the Surveyor retrorocket. The data presented on these propellants add to the extensive data obtained on other propellants elsewhere and are believed to aid one interpretation of L* instability of metallized composite propellants.

The scope of the present study includes pressure time histories in a stainless steel L* motor with metal nozzles. The troublesome blockage of such small metal nozzles with the aluminum oxide slag was minimized in these tests with the novel use of viscous silicone oil on the surface of the nozzle before each run. While the physicochemical processes behind the beneficial effect are not understood, the method has been found to be extremely effective in preventing the chamber pressure from rising steeply during a run. Also, one of the propellants tested (LS-60) has shown BMI at as high a pressure as 217 psia, thus alerting us to the possibility of high pressure occurrences of this "low pressure" phenomenon with composite propellants.

The experimental procedure is briefly described in Section II. The experimental results are presented in Section III, including a matrix of the experimental variables involved. Section IV attempts to interpret the data in terms of present concepts of L* instability. The salient conclusions and projected future work are outlined in Section V.

II. Experimental Procedure

The experiments were conducted using the facilities at JPL. The L* burner (fig. 1) is a $2\frac{1}{2}$" diameter stainless-steel cylindrical chamber that has its two ends covered with the nozzle end plate NE and the piston end plate PE. The piston end plate has passing through it a threaded rod R at the end of which is a stainless steel piston ($2\frac{1}{2}$" dia.). The propellant to be tested is bonded before each run to this piston. The pressure is sealed by the two O-rings shown at O1 and O2. The nozzle is a stainless steel piece that is machined contoured and screws into the nozzle end plate with pressure seal at O3. Nozzles of various throat diameters are available and are used interchangeably with ease. The position of the piston in the chamber determines the chamber free volume (V_c) and is preset with the use of the lock nut (L). The L* motor is mounted rigidly on a table with a 1" (heavy wall) tube stock of short length (M). The exhaust is to the atmosphere (usually 14.3 psia).

The pressure in the chamber is measured continuously during a run by one of the Teledyne

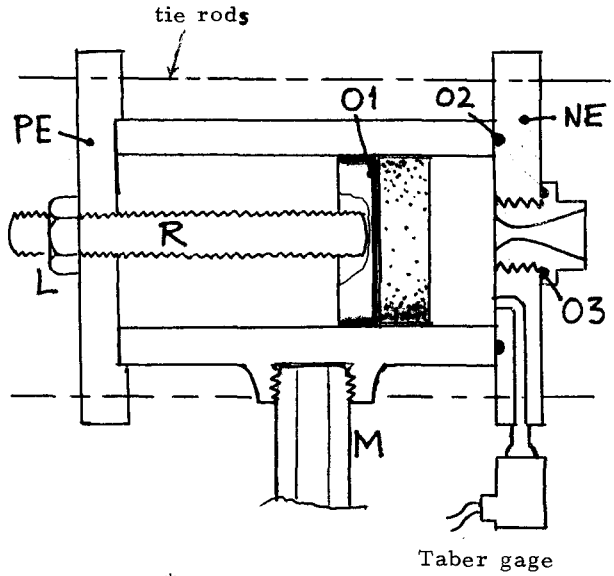

Fig. 1. The L* Burner.

Taber gages (strain gage type), different ones being used for different pressure ranges of interest. The pressure tap is a 1/8" hole that communicates with the chamber as shown in fig. 1. (Earlier runs had used a hole parallel with the axis of the chamber, but the Taber gauge at the end of the plate got in the way of mounting the burner on a vacuum manifold in those runs that used a vacuum exhaust. Comparisons of the pressure measurements with these two orientations of the pressure taps have revealed little difference in the pressure time history under otherwise similar conditions of firing. This observation is hardly surprising, since bulk mode instability is considered in the present case.) The electrical output from the gage was amplified by a Dynamics (Instrumentation Co. model 6122) amplifier and recorded on one channel of an oscillograph (either a CEC 5-124 or a Honeywell 1912 Visicorder). Since the highest frequency encountered was about 100 Hz, the frequency response of the instrumentation was not a limiting factor.

The ignition procedure employed is the one that has been found to work best both at NWC and JPL. The well-known X-225 igniter paste is applied in a thin layer over the surface of the propellant and a pellet of the X-225 (teardrop), at the center of which is the nichrome heater wire, is bonded to the center of the surface. The size of the pellet and the thickness of the surface layer can have profound influences on the nature of a run, as described earlier[18]. These two variables have to be carefully tailored to meet the requirements of each particular run. The igniter leads (copper) from the nichrome wire are led out through the nozzle and are hooked to a 28 V d.c. power supply.

In some of the runs, particularly with the TPH propellant, the need was felt for an igniter paste that would burn considerably slower than the X-225. A new paste called CIT-IP-1, which has aluminum substituted for the fine titanium in the X-225, was formulated and was found to serve its purpose rather admirably.

At the end of each run, even if the propellant was not fully consumed, the chamber free volume was determined by filling the chamber with water up to the throat of the nozzle.

In many of the earlier runs the aluminum oxide slag, from the aluminum in the propellant, continuously accumulated on the nozzle surface, and the effective throat area was thus decreasing continuously during a run. The undesirability of such a phenomenon is clearly revealed by the rising pressures, as shown in fig. 2(a). In an attempt to obviate this slag buildup, viscous silicone oil was applied on the nozzle surface before each run. In most cases, this procedure has been found to be extremely effective in reducing the slag buildup, at least for the run durations of interest in our case (usually of the order of 10 sec.). The changed pressure trace is shown in fig. 2(b).

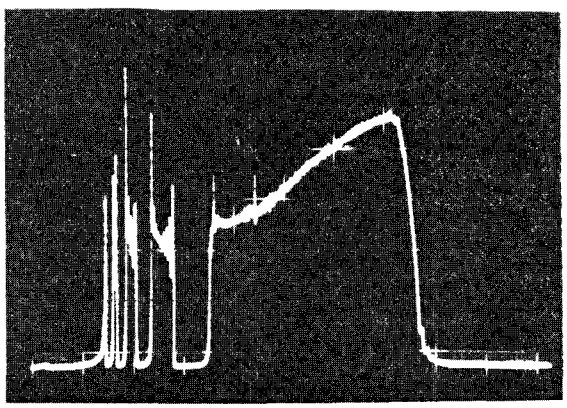

Propellant: LS-60
Metal Content: 16% aluminum
Nozzle Throat Size: 0.349" diameter

Fig. 2(a). The nozzle blockage problem.

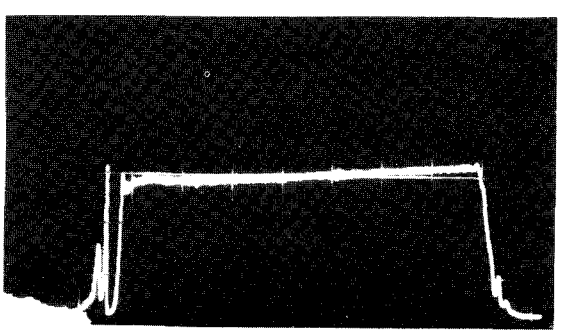

Fig. 2(b). Typical trace with silicone oil on nozzle surface with the same propellant as in Fig. 2(a).

III. Experimental Results

The experimental results were obtained on the latter three propellants noted in Table I. The $\tilde{A}$-13 propellant was not tested in the present program, but extensive data are available on this propellant from an earlier study[18, 19]. The linear regression rate vs. pressure curves obtained in a Crawford bomb under nitrogen pressure are presented in fig. 3. The propellants have the following significance. The $\tilde{A}$-13 propellant has been found to be readily unstable in many of our studies, and extensive data are available, not only in the L* burner[18, 19, 25] but also in the T-burner[26] at the higher pressures and frequencies of interest. Thus, the first modification with 2% aluminum inclusion is thought to aid data interpretation of the $\tilde{A}$-13-2A propellant. Similar propellants have of course been extensively tested elsewhere. The TPH-3274 propellant was used in the Surveyor retrorocket, and is of some practical importance. The LS-60 propellant is thought of as a possible candidate for large solid rocket boosters currently being considered for various applications.

Table 1. Propellant Compositions

	Weight Percent
1) $\tilde{A}$-13	
PBAN	20.4
Epon Resin 808	3.6
Ammonium Perchlorate ("ninety" micron)	76.0
	100.0
2) $\tilde{A}$-13-2A	
PBAN	20.4
Epon Resin 808	3.6
Ammonium Perchlorate ("ninety" micron)	74.0
Aluminum (16 micron)	2.0
	100.0
3) TPH-3274	
HC-434 Polymer, ERL-0510, Linoleic Acid	13.98
Chromium octoate (diluted, 50%)	0.02
Ammonium Perchlorate	
400 micron (spherical)	52.00
200 micron (spherical)	12.00
80 micron (ground)	6.00
Aluminum	
5 micron	8.00
30 micron	8.00
	100.00
4) LS-60	
PBAN binder system (PBAN 77 + Epon 828)	14.00
Ammonium Perchlorate (bimodal)*	70.00
Aluminum (Alcoa 1230)	16.00
	100.00

*21% no. 8 grind, 49% unground

A typical pressure trace obtained in these runs is presented in fig. 4. This represents the chamber pressure as a function of time. Because of extensive time compression, many of the details are not seen but are clearly revealed in a time-expanded oscillograph trace.

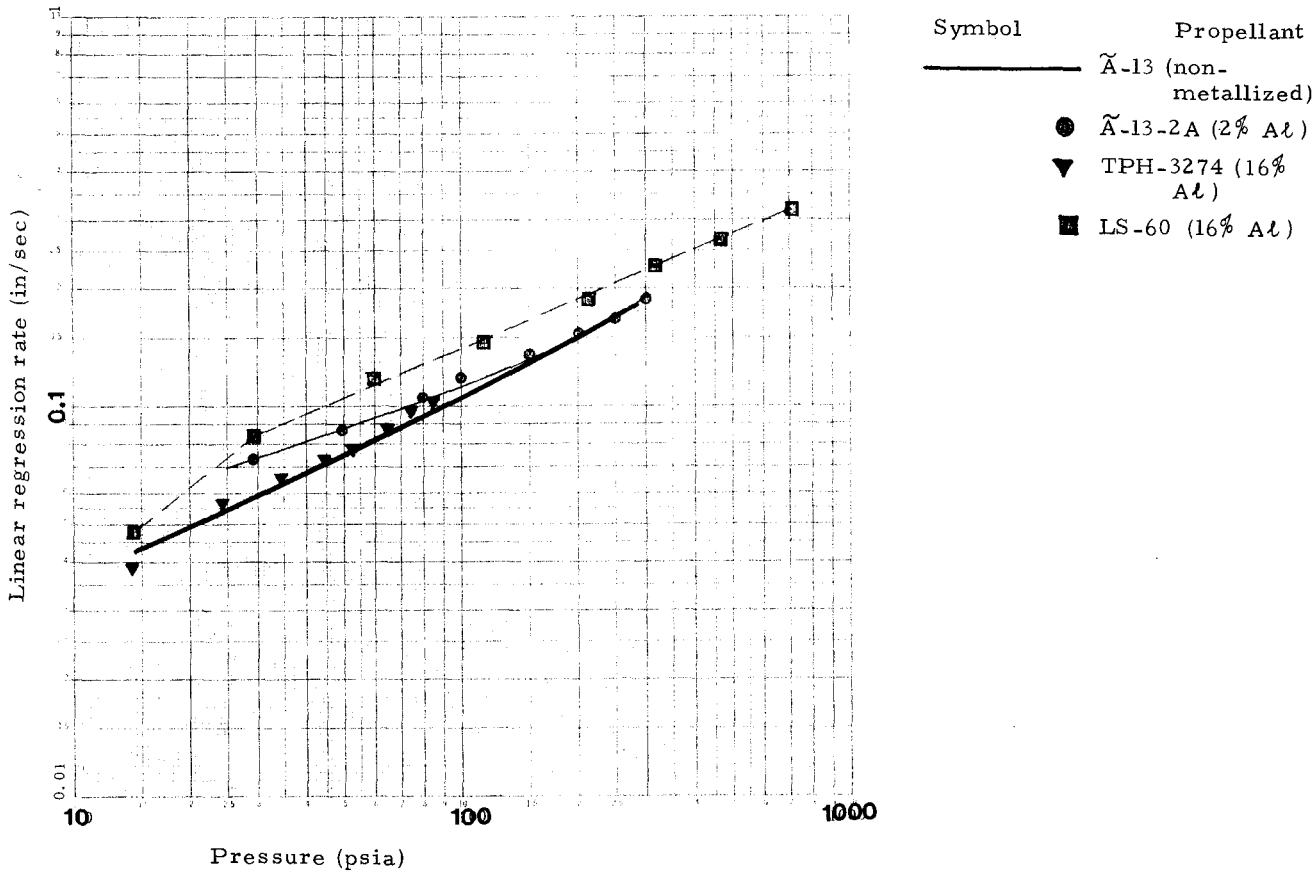

Fig. 3. Crawford bomb data on the propellants used in this study.

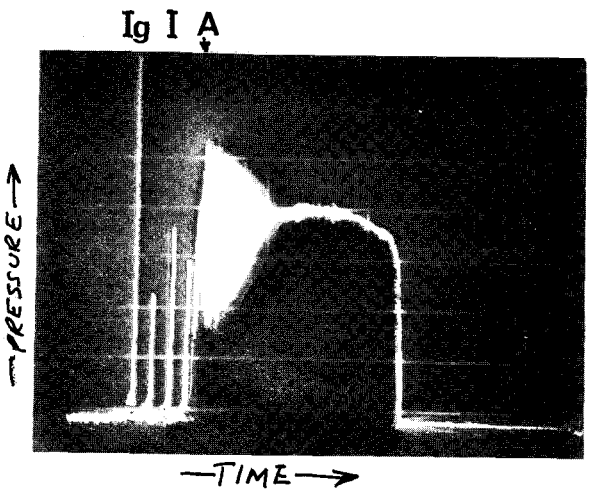

Fig. 4. Typical Pressure-Time History.

We observe the ignition "pulse" at Ig followed by some chuffs at I. As some of the propellant gets consumed, the chamber free volume (V_c) and hence the characteristic length L^* (by its definition $L^* \equiv V_c/A^*$) increases and at A, we see the establishment of a mean chamber pressure (P_c). Bulk mode pressure oscillations are superposed on the mean chamber pressure and they may grow or decay in amplitude. Point C is defined as the point at which the bulk mode oscillations merge with the general "noise" level characteristic of time-independent combustion of each propellant. With non-metallized propellants, particularly with fine oxidizer particles, the "noise" level is extremely low. But with metallized propellants, particularly with coarse oxidizer particles, the noise level is frequently very high and obscures the precise determination of the point at which the bulk mode oscillations disappear.

These features are much better seen in the time-expanded traces shown in figs. 5 and 6. In such cases, a linear extrapolation of the decreasing amplitude as it intersects the mean pressure line has been taken as the point C, i.e., the point of disappearance of the oscillations.

Contrasted with the well-defined behavior of Ã-13-2A and LS-60, the TPH propellant frequently yielded pressure traces such as the ones shown in figs. 7(a) and 7(b).

The chamber free volume which is needed to compute the characteristic length can be computed from the volume at burnout if the amount of propellant consumed at each point in time is known. Knowing the regression rate at each pressure, fig. 3, we can calculate the propellant consumption in the chamber. However, as is well known, the propellant does not obey the simple picture of linear regression during the chuff mode and care is needed in calculating the instantaneous chamber free volume V_c. The runs were usually such that either time-independent or BMI occurred near

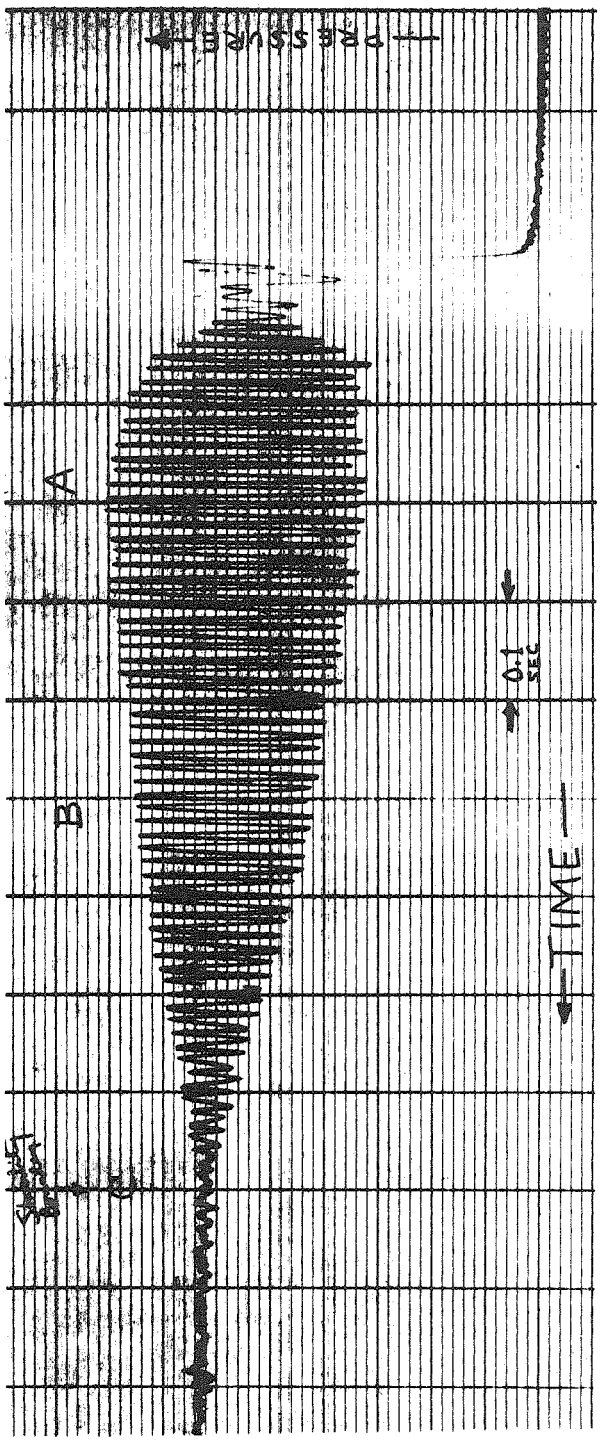

Fig. 5. Typical Pressure-Time History of A-13-2A Propellant.

burnout. Thus, the computation of the free volume was started at the burnout point and proceeded backwards in time until the desired points were computed with free volume given by

$$V_c = V_{burnout} - \frac{\pi D^2}{4} \cdot \bar{r} \times t \quad .$$

This procedure was not used in the chuff mode combustion but only during time-independent or BMI combustion.

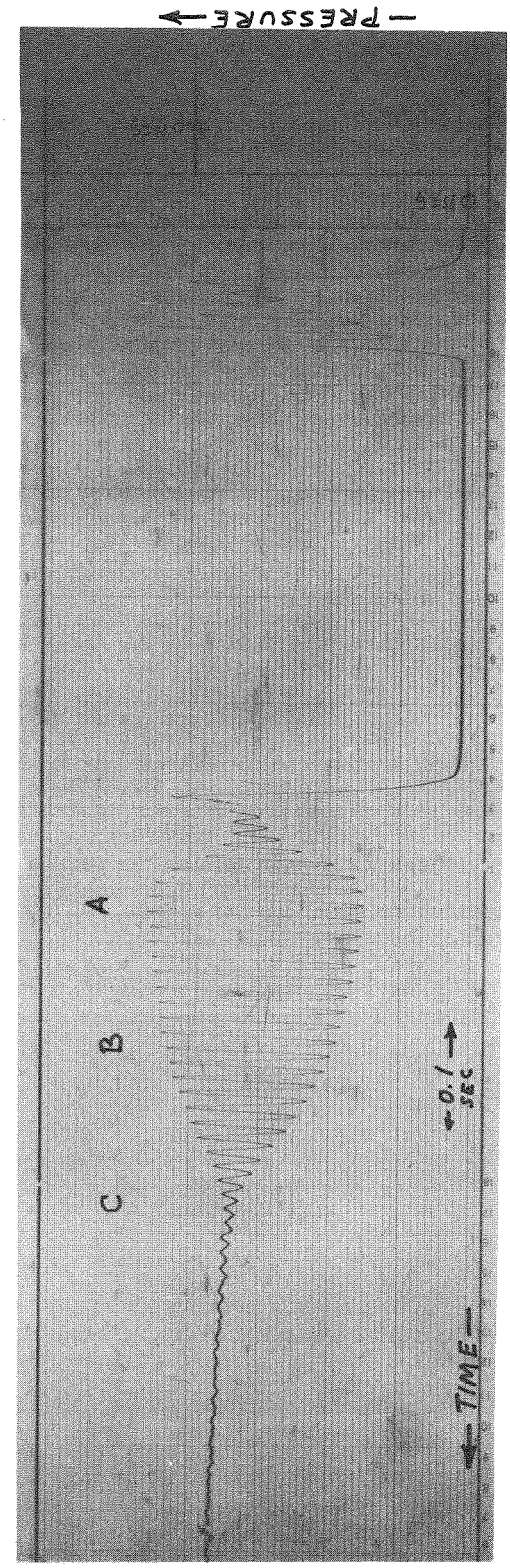

Fig. 6. Typical Pressure-Time History of LS-60 Propellant.

The experimental range of variables is indicated in Table II. All four modes of combustion were seen with these propellants.

The experimental results are presented in tabular form in Tables III - V.

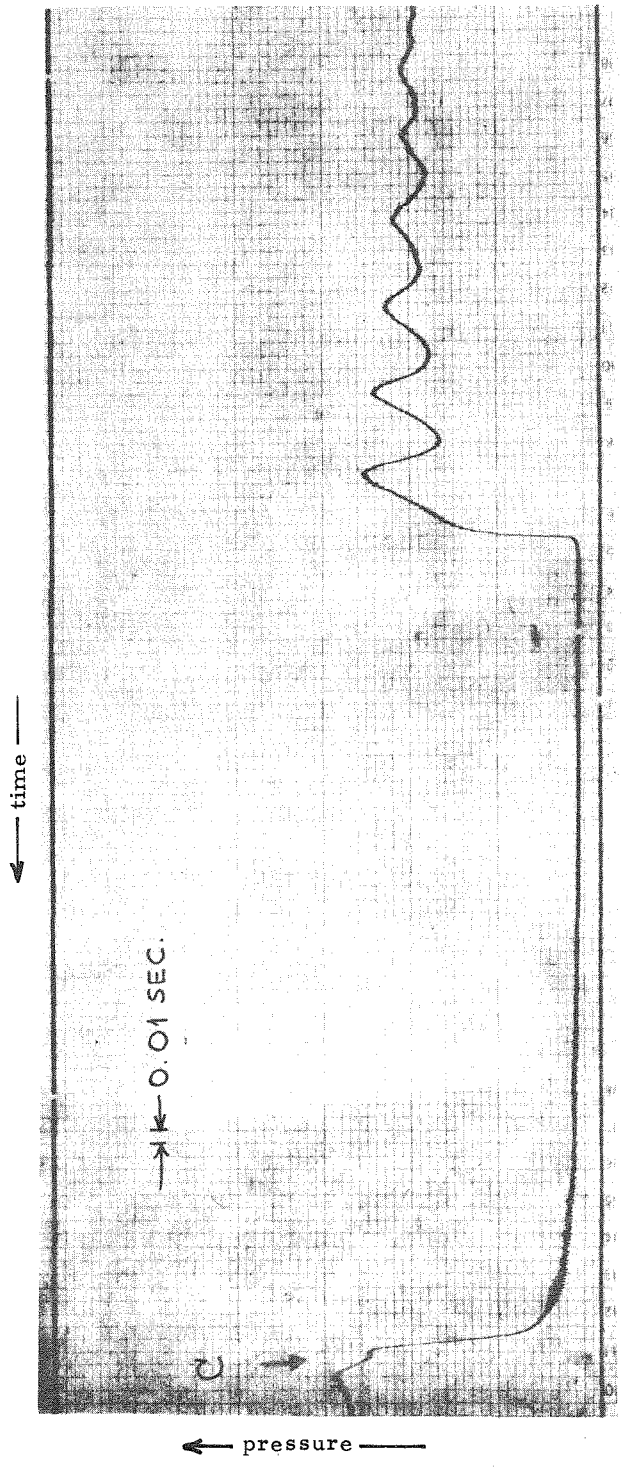

Fig. 7(a). Typical Pressure-Time History of TPH Propellant.

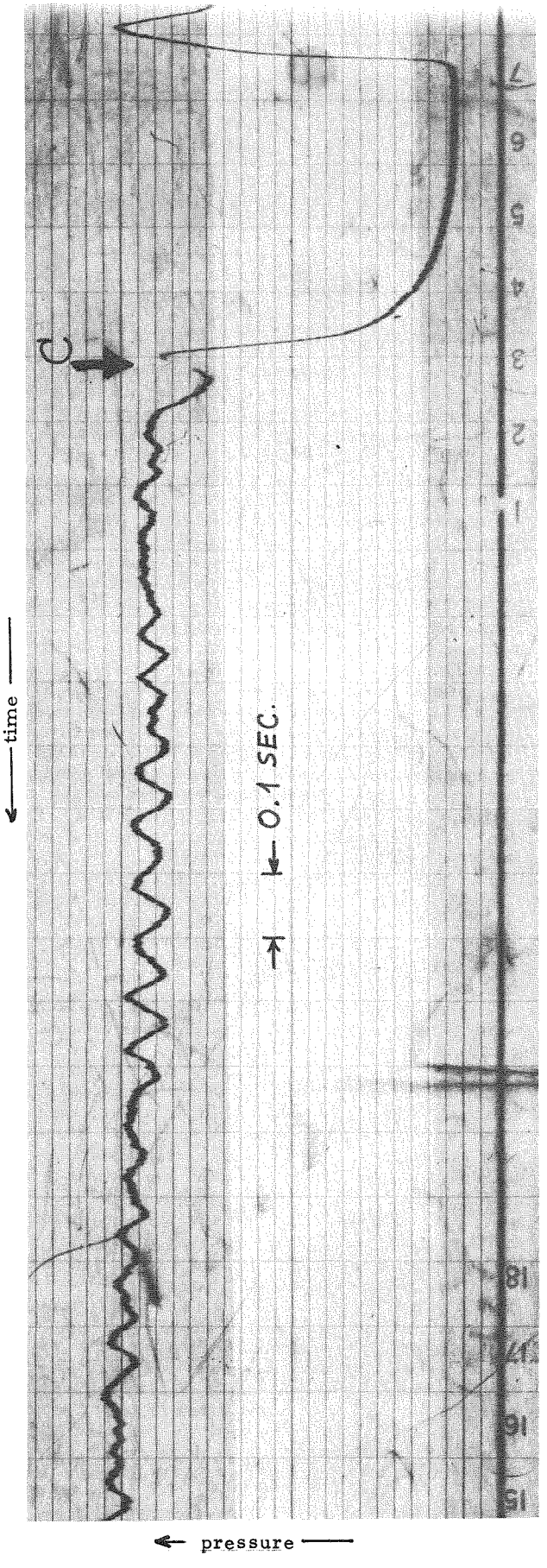

Fig. 7(b). Typical Pressure-Time History of TPH Propellant.

Propellant	Pressure Range, psia	L^* Range, cm	Frequency Observed, Hz
LS-60	35-250 (atmospheric during chuff)	5-106	20-70
TPH-3274	31-72	10-100	11-16
$\widetilde{A}$-13-2A	27-125	15-100+	45-95
$\widetilde{A}$-13 (earlier)	28-112	22-150+	36-107

Table II. Experimental Range of Variables.

The Stability Boundary

While it is obvious from pressure traces (such as figs. 5) that the motor operation goes from the unstable to the stable regime of combustion, some questions seem to have remained on the precise location of the stability boundary itself. In the strictest sense of linear analyses, the stability boundary is defined by the condition (the growth constant for infinitesimal disturbances) $\alpha_g = 0$. Hence, a plot of α_g extrapolated to $\alpha = 0$ axis may determine the boundary at various values of L^* and P. Another way is to map the regions of stable and oscillatory burning in discrete firings. Yet another way is to recognize that in the linear regime, the amplitudes are assumed to decay exponentially in time in the stable regime. Hence, the point at which an exponential decay appears may be taken as being very close to the stability boundary. In the present case, it has been taken in the past[8,10] that the point A (in pressure traces such as fig. 5) is the stability boundary, since the point A represents the boundary between growing and decaying pressure oscillations. However, the decreasing pressure amplitude seen in the segment A-C is not in a stationary system. The chamber characteristic length is varying in time because of propellant consumption. In fact, the propellant burns at a constant rate at a given pressure, and hence the chamber free volume is increasing linearly in time in the regime AC.

The decay of pressure amplitude is also linear in time and not exponential, and is thought to correspond with this linear change in L^* with time. Hence, although the pressure amplitude is decreasing in time, the regime of operation appears to be still unstable. Thus, the point C where the pressure amplitude merges with the "noise" level in time-independent combustion is taken as the stability boundary. Even when the starting points (i.e., points such as A in fig. 4) are different, which is achieved either through the use of propellants of different initial thickness or through a different initial setting of the piston position, the oscillations have been seen to disappear at the same points, such as C, within experimental error.

In some other instances the determination of the stability boundary was not so straightforward. For example, as shown in fig. 7(a), a period of chuffing or BMI with a resulting (dp/dt) "extinguishment" was followed by time-independent combustion. In such cases the point at which the time-independent combustion started is taken as the stability boundary [C in fig. 7(a)]. This follows from the definition that the stability boundary isolates regions of stable and unstable motor operation.

Frequency of Oscillations

It is a very straightforward procedure to compute the frequency of oscillations from the pressure-time history. The determination of the values of L^* at each location is not so simple, particularly when the location of interest happens to be the middle of a chuff or isolated by periods of no apparent activity. This is because the amount of propellant consumed during such phases of operation is undetermined, at least in the present study. However, wherever the L^* could be determined with a fair degree of certainty, the frequency is reported as a function of L^* in the tables.

The stability boundaries for the propellants are presented in figs. 8, 9, and 10, and the frequency is presented as a function of L^* for all three of the propellants in fig. 11.

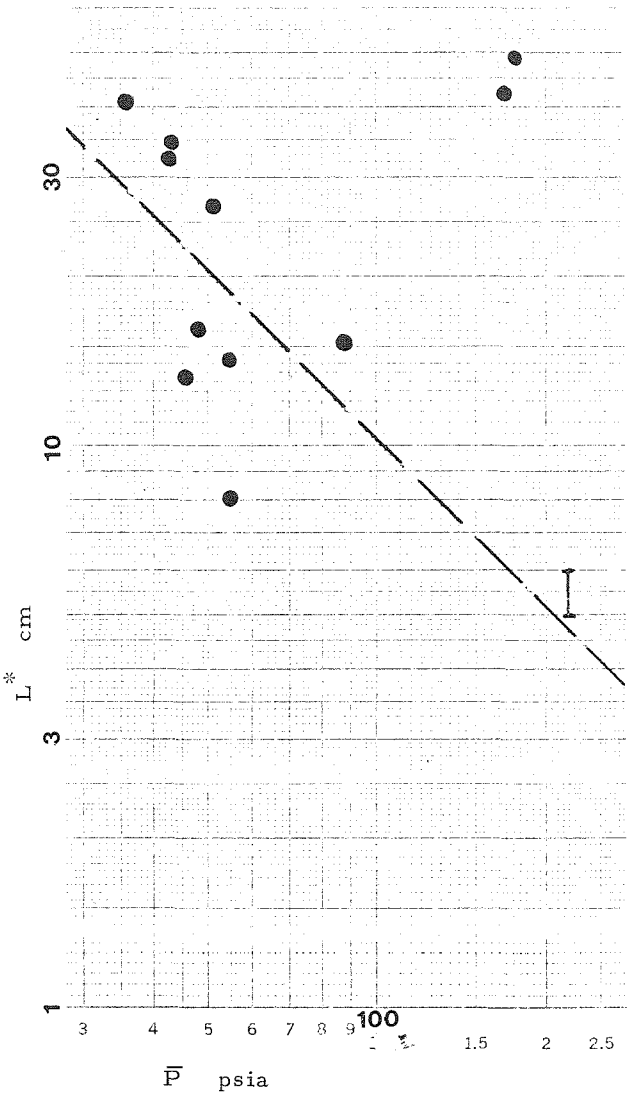

Fig. 8. Stability Boundary of the LS-60 Propellant.

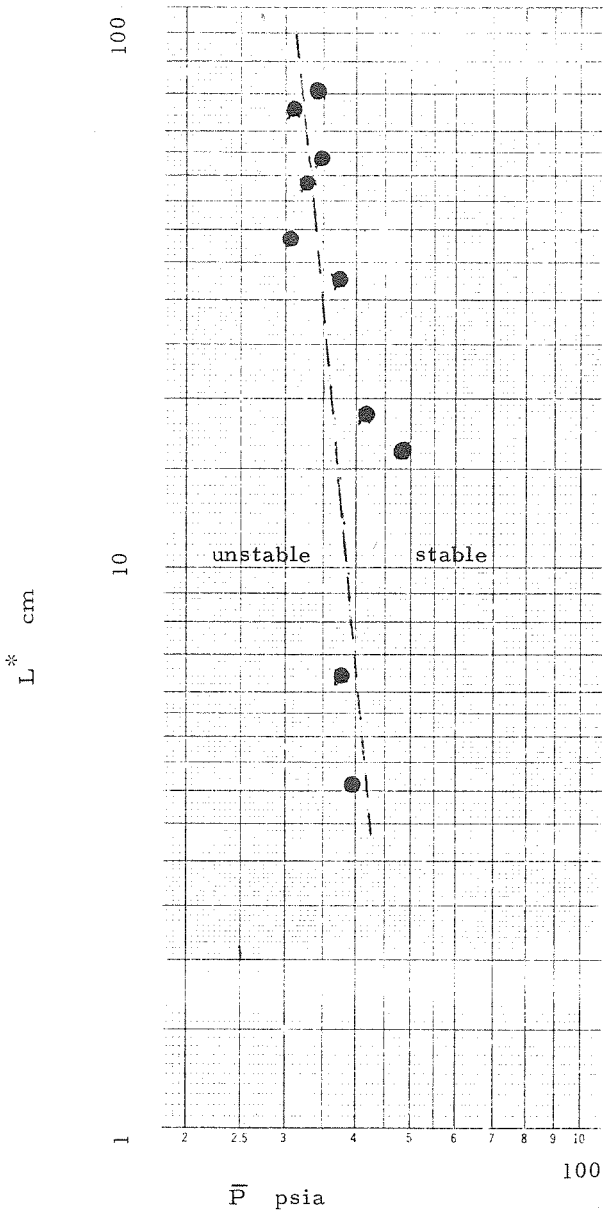

Fig. 9. The Stability Boundary of the TPH-3274 Propellant.

IV. Interpretation and Discussion

The two popular aspects of L^* instability, namely the stability boundary and the frequency of BMI, are discussed below. (As was mentioned previously[18, 19], the limiting pressure amplitudes during BMI have not been well correlated so far. This aspect is probably so nonlinear that simple treatments are not meaningful. In any case, the extensive coverage of the limiting amplitudes in a much simpler non-metallized system[18, 19] and the non-emergence of a satisfactory explanation, coupled with the fact that the limiting amplitudes do not normally receive in the literature the same importance as the frequency, etc., have all contributed to the present reluctance to discuss them.)

The Stability Boundary

The LS-60 propellant has indicated (fig. 8) a stability boundary that is normally accepted as the

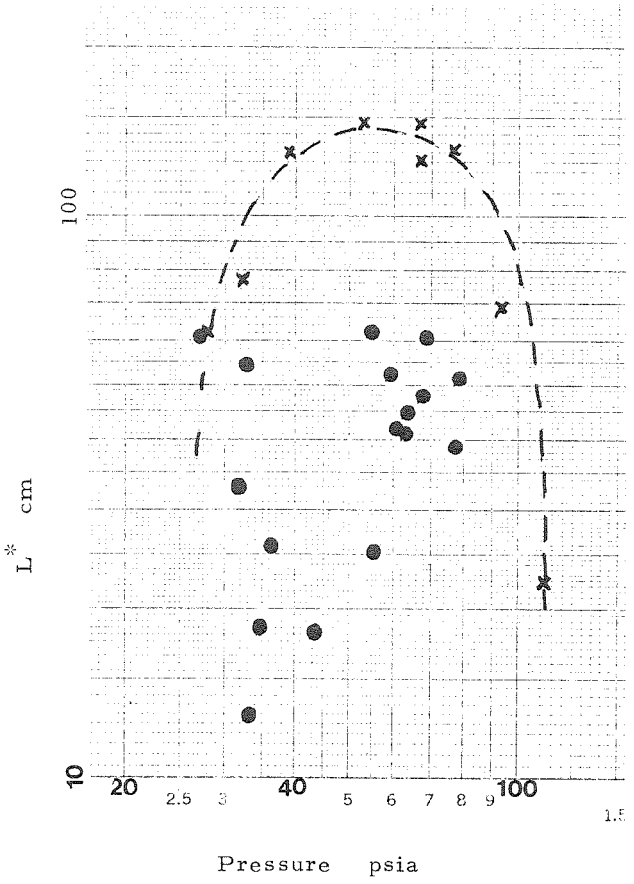

Fig. 10. The Stability Boundary of the $\widetilde{A}$-13-2A Propellant (●) and Comparisons with the Earlier $\widetilde{A}$-13 Data (✖).

observed shape[8, 15]. The points on the log-log plot appear to be well correlated by a straight line except for the two data points around $\bar{P}$ = 180 psia and L^* = 45 cm. These two data points are among the best obtained, and it is hard to ascribe them to experimental error. Some further experiments in that regime may be of value in determining the exact behavior of the propellant.

If any errors occurred at all in the computation of the value of L^*, they are likely to move these points farther away from the general trend in that the L^* values may be a little higher due to any nozzle coating, due to aluminum oxide slag. Although the nozzle blockage was very little, as evidenced by the pressure-time histories, a small decrease in throat size can not be ruled out, and the effective L^* value would consequently be higher. The slope of this boundary appears to be much less than what has been seen sometimes with a high percentage of aluminum in propellant formulation[15]. However, the data of Beckstead[8] on the XF propellant (10% aluminum) indicates a slope of the same general value as has been obtained here. This seems to indicate that the binder system is probably important in determining not only the slope of this curve but also its variations with aluminum contant. Strand[15] used the polyurethane system and found that the boundary became progressively steeper as the aluminum content varies from 0% to 16%. The other data[7] indicate that the slope of the dp/dt extinction curve on the L^*-$\bar{P}$ plot is not much affected as the aluminum concentration is increased

Table III. Experimental Results on the Ã-13-2A Propellant

Run No.	Nozzle Throat (inch)	L^* at Burnout (cm)	Large Amplitudes (Point A) or Start $\bar{P}$ (psia)	L^* (cm)	f (Hz)	$\lvert P' \rvert$ (psig)	Intermediate Amplitudes (Point B) $\bar{P}$ (psia)	L^* (cm)	f (Hz)	$\lvert P' \rvert$ (psig)	Stability Boundary (Point C) $\bar{P}$ (psia)	L^* (cm)	f (Hz)
268	0.312	123.5	38.4	---- time-independent combustion ----------									
269	0.312	83.0	36.0	---- chuff followed by time-independent combustion ----------							36.0	25.7	
271	0.386	70.1	---------- -- chuffing combustion only ----------										
272	0.386	51.7	---------- chuffing combustion only ----------										
273	0.349	61.5	27.65	----	62.5	----------	60-61	45	3.45		27.0	61.0	
274	0.349	38.75	----------				28.1	38.75	62	5.45	31.2	33.0	
275	0.349	61.4	---------- chuffing followed by time-independent combustion ---------								32.6	54.2	
276	0.327	72.0	31.75	----- chuffing followed by time-independent combustion ---------							34.1	18.3	
277	0.327	66.4	31.45	----- chuffing followed by time-independent combustion ---------							32.98	12.85	
278	0.312	66.8	37.1	----- chuffing followed by time-independent combustion ---------							36.5	6.98	
279	0.298	81.0	---------- chuffing followed by time-independent combustion --------								33.0	18.3 *	
280	0.272	90.9	60.4	27.8	75	----------					60.4	41.4	
281	0.272	92.2	53.8	15.1	85.75	24	----------				55.0	25.2	83.4
282	0.272	90.9	62.8	16.9	95	39.4	48.5	32	75.7	27.4	62.8	40.5	70
283	0.262	114.6	55.8	40.75	71.5	20.4	40.8	46.875	66.6	16.05	58.8	52.5	66.6
285	0.25	123.1	52.1	39.2	66.6	39.5	39	51	66.6	23.65	54.5	62.8	71.0
288	0.237	21.15	94.3	21	95	---- (dp/dt) extinguishment ----------							
289	0.237	137.2	106.6	------- time-independent combustion ----------									
290	0.223	151.0	124.5	------- time-independent combustion ----------									
292	0.223	134.9	113.6	---------- time-independent combustion ----------									
293	0.237	130.1	103.3	---------- time-independent combustion ----------									
300	0.25	104.0	71.6	20.6	80	46.5	74.1	29.7	71	29.7	76.55	38.8	75
301	0.262	117.5	71.9	---------- time-independent combustion ----------									
302	0.262	25.8	67.5	25.8	70	53.2	--------- (dp/dt) extinguishment ----------						
303	0.262	106.3	68.1	36.9	68	44.7	68.1	48.5	65	31.4	68.1	60.1	66
304	0.262	100.9	61.5	33.6	80	24.15	62.1	39.6	76	10.875	62.7	45.6	75
305	0.262	109.0	77.5	32.9	72	30.3	77.5	39.05	70	18.15	77.5	51.0	69
306	0.262	100.9	64.55	24.95	75	38.65	66.475	36.35	70	31.4	67.4	47.75	70

Table IV. Experimental Results on the TPH Propellant.

Run No.	D^* (in.)	Starting Point $\bar{P}$ (psia)	Starting Point L^* (cm)	Intermediate Point (Stability Boundary) $\bar{P}$ (psia)	Intermediate Point (Stability Boundary) L^* (cm)	Intermediate Point (Stability Boundary) f (Hz)	Burnout $\bar{P}$ (psia)	Burnout L^* (cm)
210	0.312	33.98	9.91	48.25	16.22	--	52.68	50.68
211	0.312	41.05	very small	41.05	18.51	15.4	49.81	38.52
212	0.327	44.32	very small	38.97	4.06	--	39.79	33.22
217	0.327	37.48	36.61	34.3	70.61	11.1	34.3	92.28
225	0.338	31.76	17.85	32.72	48.87	11.1	28.65	69.96
231	0.312	32.23	11.83	36.92	32.74	12.5	51.64	72.99
32	0.312	36.43	1.8	37.66	6.43		71.68	62.85
233	0.327	43.60	very small	34.6	53.52	--	34.6	53.52
235	0.327	34.64	34.76	31.17	65.46	11.1	35.13	90.44
239	0.349	30.04	4.59	30.66	38.59	--	33.44	53.47

Table V. Experimental Results on the LS-60 Propellant.

Run No.	D^* (in.)	Starting of the Large Amplitude Region $\bar{P}$ (psia)	L^* (cm)	f (Hz)	Intermediate Region "C" in the Stability Boundary $\bar{P}$ (psia)	L^* (cm)	f (Hz)	Burnout Region $\bar{P}$ (psia)	L^* (cm)	f (Hz)
246	0.375	41.81	13.8		36.98	35		35.49	56.1	
247	0.375	35.95	64.3		35.94	85.4		37.06	106.6	
248	0.349	33.05	50.8		48.68	52.35		44.3	99.7	
249	0.349	42.71	11.1	23	48	16.16 (C)		51.19	60	
250	0.349	43.74	4.6	32	51.8	26.5 (C)	60	72.77	53.5	
251	0.349	45.37	3.0	30	45.61	13.21 (C)		69.54	51.9	
252	0.327	46.99	very small	33	54.81	8 (C)		105.33	64.6	
253	0.338	60.58	very small		36	40.8 (C)		23.87	68.2	20
254	0.338	46.52	11.8	30	54.3	14.11 (C)		62.08	63.9	
255	0.375	26.68	1.2		43.11	34.3 (C)		57.16	43.5	
256	0.375	33.44	very small		42.7	32.1 (C)	22.8	40.53	42.1	
257	0.298	84.20	very small		87.12	15.4 (C)	60	119.88	66.7	
								Point (B)		
258	0.272	155.3	25.85	65	171.3	42 (C)	65	157.6	33.93	65
259	0.262	176.3	28.15	62	176.3	48.5 (C)		176.3	38.33	62
260	0.25				217.5	5-6 (C)	70			
270	0.386	chuffing combustion only								

from 0% - 16% in the UTREZ binder system. This extinction curve on the L^*-$\bar{P}$ plot should bear a relation to the stability boundary on the same L^*-$\bar{P}$ plot and hence the data are of relevance here also. (Usually, in a given propellant, higher frequencies are associated with lower L^* values. Higher frequencies imply higher dp/dt values. Thus, the dp/dt ordinate may be looked upon as an inverse L^* ordinate. This argument is crude and assumes, for example, that $|\dot{P}'|$ is of the same order of magnitude as the L^* varies. But the general conclusions from this certainly seem to be valid, as may be seen in ref. 15.)

The stability boundary for the TPH propellant shown in fig. 9 is also in agreement with the generally accepted shape of such a boundary[8, 15]. The line is very steep and clearly indicates that the details of a propellant formulation are very important in determining its stability characteristics even in the simple L^* mode. (For example, the LS-60 and TPH propellants both have polybutadiene backbone in the binder. The LS-60 employs PBAN and the TPH, CTPB. Both of these propellants use 16% aluminum.)

The $\tilde{A}$-13-2A propellant is particularly important in the present studies since the propellant is formulated to be a minor variation of the earlier[18, 19] $\tilde{A}$-13 propellant. As can be seen in fig. 10, the stability boundary could not be well defined during these tests. For comparison, the earlier data on the $\tilde{A}$-13 propellant are also presented.

Several questions arose with regard to the $\tilde{A}$-13 propellant, particularly regarding the parabolic shape of its stability boundary. Since the presentation of the earlier data[19], some tests were repeated with the $\tilde{A}$-13 propellant in the low pressure segment of operation. The results once again indicated stable operation at low pressures and small L^*. Thus, the parabolic shape of the stability boundary for the $\tilde{A}$-13 propellant is consistently seen in our experiments. The stability boundary points of the $\tilde{A}$-13-2A propellant are practically all within the earlier parabola (fig. 10). Also, the propellant has indicated time-independent combustion at values of L^* and mean pressure at which the $\tilde{A}$-13 propellant operated in the BMI or chuffing regime.

There is a general agreement in the literature[1, 6, 7, 8-12, 15] that the addition of aluminum tends to make a propellant more unstable in the L^* mode. This is not seen in the present experiments with $\tilde{A}$-13-2A. The experimental data were generally of the quality shown in figs. 4 and 5. As can be seen, possible improvements in our experimental technique are unlikely to alter the basic conclusion that the $\tilde{A}$-13-2A propellant is more stable than the $\tilde{A}$-13 propellant, at least in the range tested. It is possible that a propellant with 2% aluminum represents an "insignificant" change from a 0% aluminum propellant and cannot be used as a basis for definite statements regarding stability trends. The same 2% aluminum addition in the polyurethane[15] system seems to have indicated a shift towards greater instability, although it is a very small shift[15] indeed. More testing with the same propellant along with its next successive change (4% aluminum in $\tilde{A}$-13) may help to resolve the issue.

It is mentioned in the literature that accumulation of aluminum on the propellant surface resulting in "periodic shedding" of the aluminum, because of inefficient combustion at low pressures, probably aggravates the L^* instability problem. The frequency of such a periodic shedding would also be low and might match with the low frequencies naturally prevalent in the L^* mode instability. In the present case, no such periodic shedding has made itself evident in the pressure traces, and could account for the non-aggravation of the L^* instability. The polyurethanes are known to melt readily, and a natural melt layer on the surface of the burning propellant may make a difference in the behavior of even small concentrations of aluminum (like 2%).

Frequency of BMI

As seen in fig. 11, the frequency of the $\tilde{A}$-13-2A and TPH propellants form two rather well defined regions. The case of the LS-60 propellant is interesting, in that it seems to follow two separate frequency bands. The best fit line through the earlier data on the $\tilde{A}$-13 propellant is also presented in fig. 11.

For a given oxidizer particle size in the propellant formulation, such simple bands have indeed been observed in the past, at least for monomodal distributions. The addition of metal does not seem to contradict this general trend. The frequency of oscillations was argued[14, 19] to be strongly influenced by the oxidizer particle size. Thus, with bimodal oxidizer particle sizes, it is natural to expect two principal frequencies. In fact, such

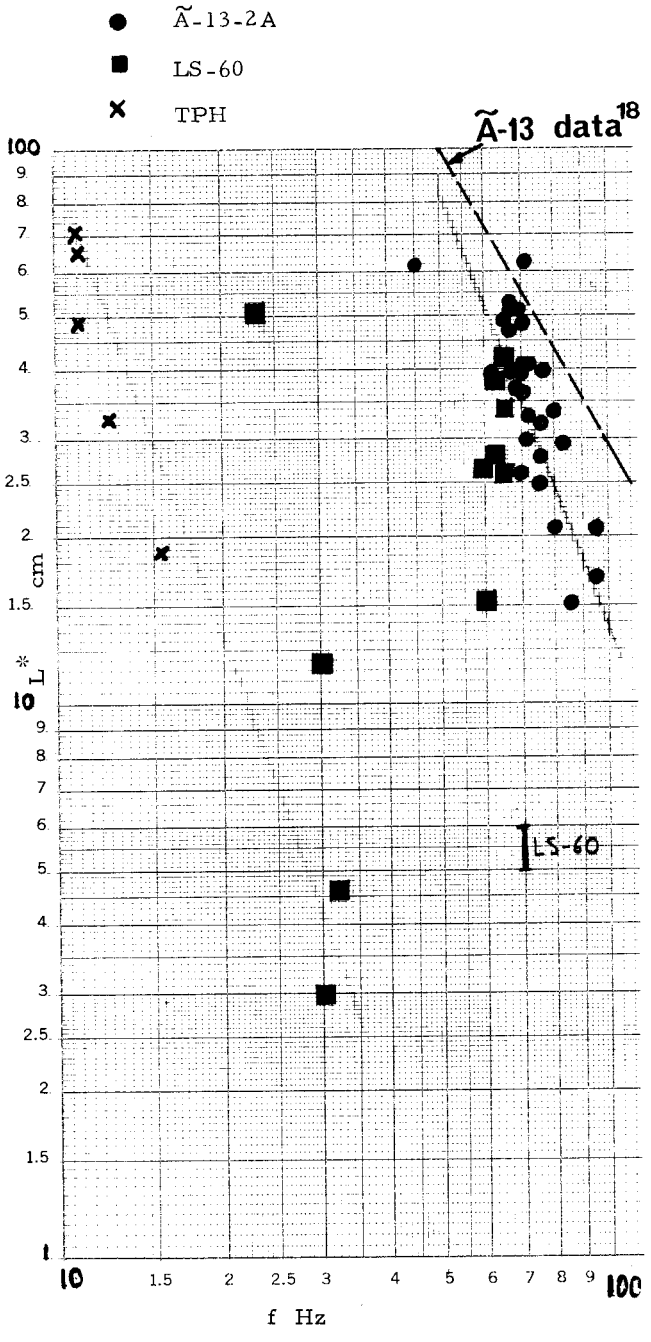

Fig. 11. Observed Frequencies of BMI Oscillations

"dual frequency" oscillations have indeed been seen during the course of a single experiment[14].

At this stage a digression is necessary to clearly understand the nature of the oxidizer particle size referred to in the industry. Typically, the oxidizer particle size is determined by the plot of the size (in microns) versus the precent-weight-less-than in the distribution. A typical distribution is shown in fig. 13. This is the blend used in our $\tilde{A}$-13. The distribution is popularly known as ninety micron AP, although it is readily appreciated that 90μ represents neither the 50 % nor the 100 % wt. average point! In our previous work[18] it was found that the 100 % weight average point (a_{100}) was far more significant than the 50 % weight average

point (a_{50}). Hence, in all of our discussion we refer to a particle size by its a_{100} in microns. The "unground" AP in LS-60 has its $a_{50} = 175\mu$ and $a_{100} = 335\mu$. The "No. 8 grind" AP in LS-60 has $a_{50} = 11\mu$ and $a_{100} \cong 43\mu$. The "Ninety" micron AP used in $\tilde{A}$-13 and $\tilde{A}$-13-2A has $a_{50} = 39.5\mu$ and $a_{100} = 100\mu$.

The frequencies seen with the TPH propellant probably correspond to the coarser oxidizer particle sizes. Simple scaling rules are not available to confirm this speculation. The two principal frequency bands seen with the LS-60 do not seem to directly scale with the oxidizer particle sizes in its bimodal blend. (7.8 is the ratio of coarse to find oxidizer sizes and the frequency ratio is more like 2 - 2.5.) The scaling rule developed in ref. 14 for bimodal blends was for non-metallized propellants, and generalizations to propellants having as high as 16% aluminum are not clear. In fact, the frequency of the LS-60 propellant correlates much better with the thermal depth scale $(\kappa/\bar{r})$, i.e., with the standard normalization $\Omega \equiv (f\kappa/\bar{r}^2)$ in fig. 14. Such a normalized variable was not successful in correlating the data on propellants using monomodal distribution of AP as discussed in detail in ref. 18. Thus, it is tempting to speculate that the thermal depth scale has an influence on the frequency of BMI when the condended phase heterogeneity cannot be well defined, either because of multimodal distribution of particle sizes or because of heavy concentrations of aluminum. (Incidentally, a thermal diffusivity value of 11×10^{-4} $cm^2 sec^{-1}$ has been consistently used for all of our propellants. Its value is not precisely known; but its precise value is not crucial for our purposes, since it enters only as a scale factor in our calculations.)

The frequency data on the $\tilde{A}$-13-2A propellant show the general trends observed earlier with the $\tilde{A}$-13 propellant. In our earlier study, the following normalized variables were found to correlate well the frequency data on four different propellants,

$$f \cdot \frac{a_{100}}{\bar{r}} \quad \text{and} \quad L^* \frac{\bar{r}}{\kappa} \quad .$$

The arguments behind these scales are fully discussed in ref. 18. Briefly, the $f\, a_{100}/\bar{r}$ normalizes the observed frequency with the "layered" frequency in the condensed phase, i.e., the frequency of the surface passing one layer of the oxidizer particles. The characteristic length normalized by the gas phase flame standoff distance leads to $L^*\bar{r}/\kappa$. [It should be recognized that we are not correlating $\bar{r}$ vs. $1/\bar{r}$. For example, the other correlation suggested by Beckstead[10] was $4\kappa\omega/\bar{r}^2$ vs. $L^*/(C^*\bar{r}^2/4\kappa RT_f)$ which is obviously not a correlation of $1/\bar{r}^2$ vs. $1/\bar{r}^2$.] Such a plot is presented in fig. 12. Earlier data on the $\tilde{A}$-13 propellant is shown along with the best-fit line drawn through the earlier data on four different propellants[19]. It is seen that the $\tilde{A}$-13-2A data seem to be an extension of the $\tilde{A}$-13 data although rather away from the general trends of overall behavior of non-metallized propellants studied earlier. The presence of 2% aluminum is seen to shift $L^*\bar{r}/\kappa$ to lower values. Otherwise, a correlation is unmistakable in this group of variables.

With the inclusion of aluminum in the propellant, the flame standoff distance is likely to be higher than with its non-metallized counterpart.

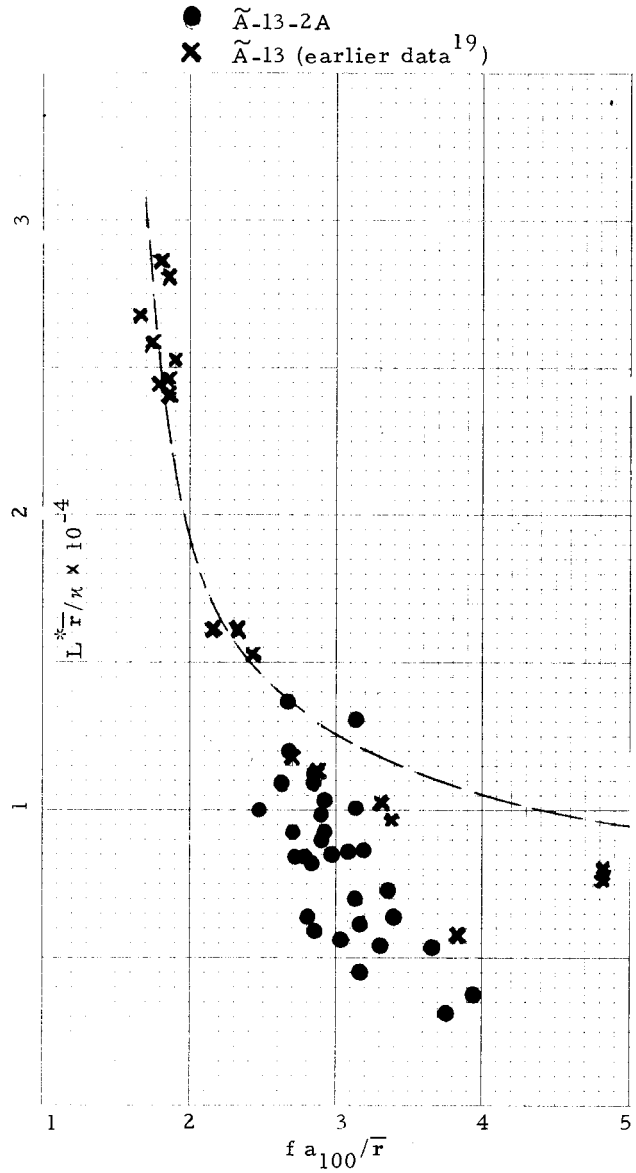

Fig. 12. Normalized frequency vs. normalized L^*. $\tilde{A}$-13-2A data compared with earlier $\tilde{A}$-13 data.

The scaling resulted from assuming that the flame standoff distance X^* was proportional to u_g. That is, $X^* = (\text{A constant}) \cdot u_g$. The value of this proportionality constant is likely to be higher for metallized propellants. Thus, the value of the ratio L^*/X^* is likely to be lower than what has been assumed for the $\tilde{A}$-13 propellant and carried over without change to the $\tilde{A}$-13-2A case also. More experimental observations are needed to quantitatively confirm this point, but the argument is consistent with our general picture of metallized composite propellant combustion. It is thus seen that some features of aluminum combustion may be necessary to satisfactorily explain the data. While 2% aluminum addition did not make its presence felt in our L^* studies, either through its "destabilizing effect at the low pressures and frequencies" or through the "periodic shedding" process, its simple combustion effects in the gas phase may well control some of the observed frequency vari-

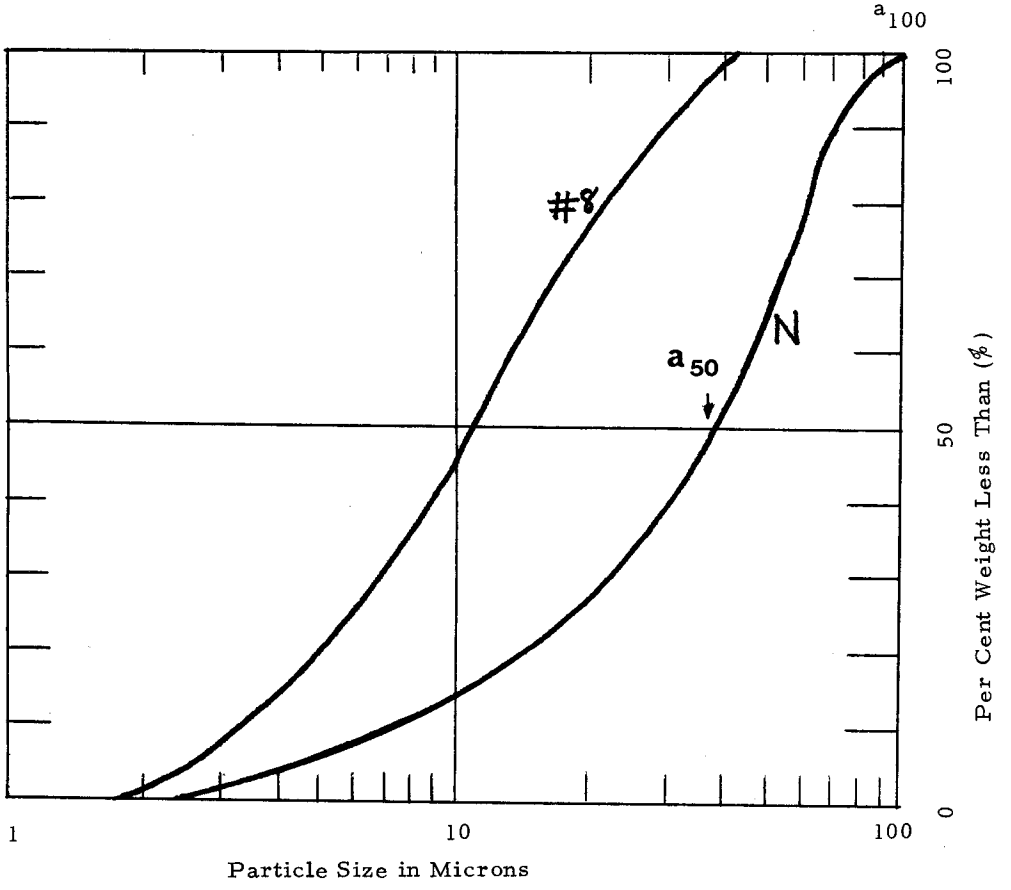

Fig. 13. Two of the AP particle sizes used in our study. #8 is the "#8 grind" used in LS-60, N is the "Ninety Micron" AP used in Ã-13-2A.

ations with L^*. Thus, we arrive at the interesting possibility that the L^* instability research may actually aid us in our studies of distributed gas phase combustion with the metallized propellants at low pressures.

V. Conclusions and Future Work

The present experiments on metallized propellants and comparisons with our earlier data on non-metallized propellants have yielded a variety of data that support the following general statements. Some of these conclusions are not new either to metallized propellants or to L^* instability, but the others are thought to be new. In any case, the data obtained should aid the interpretation of propellant behavior and L^* instability, and hence should be of value in any theoretical treatment of this phenomenon.

The stability boundaries of the heavily metallized TPH and LS-60 propellants are of the same general shape as has been reported for other propellants elsewhere. But the case of the mildly metallized Ã-13-2A is not so certain. The parabolic shape of the stability boundary of its non-metallized counterpart (Ã-13) is consistently seen, and the inclusion of 2% aluminum in place of AP seems not to aggravate the L^* instability. The quality of experimental data obtained as seen both in the pressure trace and in the frequency data indicates that improvements in the experimental technique are unlikely to alter these fundamental observations. Such small concentrations (2%) of aluminum seem to depend for their influence on the nature of the binder system in the propellant.

In this respect, a melting binder (PU, for example) may give a very different result from a non-melting binder (PBAN, for example). Also, no direct evidence is available of the periodic shedding frequency or associated effects with the 2% aluminum addition to Ã-13.

The BMI frequency of highly metallized composites employing multimodal AP distributions is probably more readily understandable in terms of the thermal depth in the condensed phase than in terms of the condensed phase heterogeneity (oxidizer particle size). This may be because of the presence of molten aluminum on the propellant surface, which may obscure the particle size effects (which are not well defined anyway with multimodal AP distributions). The BMI frequency of the Ã-13-2A propellant shows a decrease in value from the non-metallized Ã-13 at similar values of L^*. The frequency definitely scales with the oxidizer particle size and seems to form a logical extension on the normalized curve of frequency vs. characteristic length. Whether this is due to the small concentration of aluminum or due to the monomodal distribution of AP is not certain at this stage, but is probably due to the former. The next series of experiments with 4% and 8% aluminum in Ã-13 (in place of AP) should answer this question in more certain terms. Also, the frequency correlation technique has indicated that the gas phase combustion zone may have important influences over the L^* instability behavior with metallized propellants, an effect not apparent with the non-metallized propellants tested earlier[18, 19].

Composite propellants can show BMI at much higher pressures than what is normally thought of

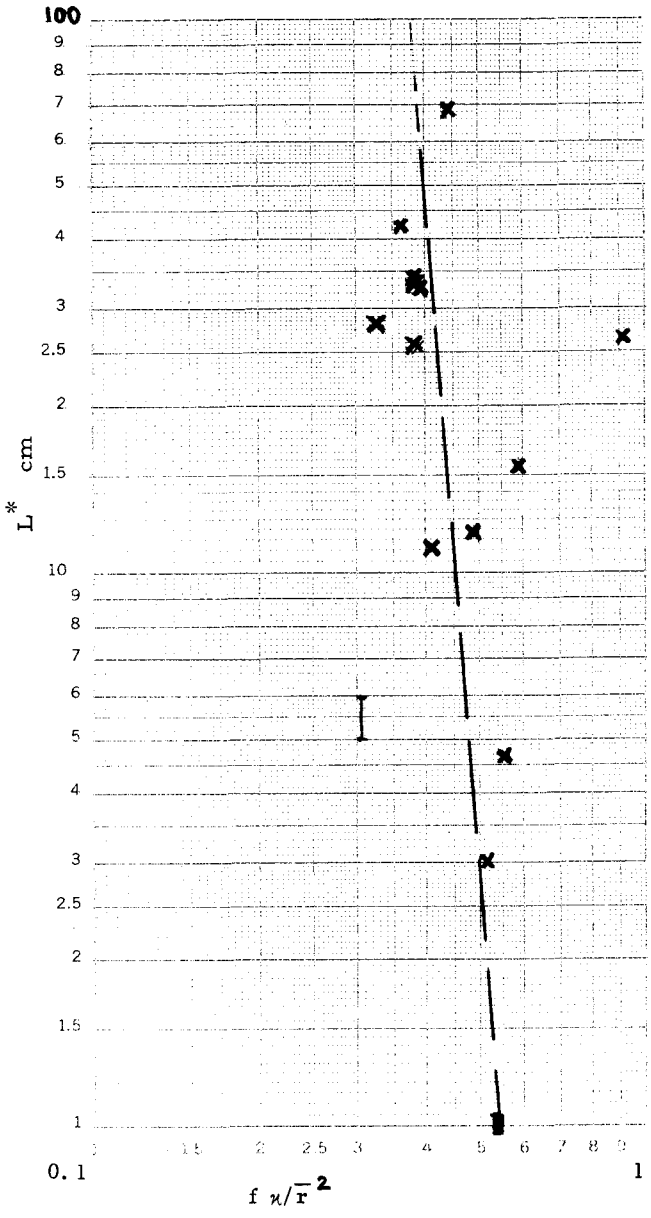

Fig. 14. Frequency data on the LS-60 propellant normalized with respect to the thermal time.

($\lesssim$ 100 psi) as their L^* instability domain.

Silicone oil on the nozzle surface is effective in preventing the slag buildup on small metal nozzles, at least for short durations. This beneficial effect is probably due to decreased heat transfer to the metal nozzle. The effect appears to be physical and not chemical; use of silicone grease was not effective in preventing nozzle buildup. Liquid propellant researchers have reported[27] greatly reduced heat transfer to inert surfaces with small percentages of silicone compounds included in the propellants. Similar techniques are being considered in solid propellants also. Propellants will be formulated with silicone compounds in them and the effect on heat transfer to inert surfaces will be determined. Loss in propellant performance (I_{sp}) will also be determined. Compounds in propellant formulation to combat heat transfer may soon enjoy the same status of compounds that are presently used for mechanical property improvement. The possible overall economy is self evident.

Acknowledgments

This work was supported by NASA under the Jet Propulsion Laboratory Contract NAS 7-100 through a Caltech work order (no. 61496). The author is very grateful to the Solid Propellant Engineering Section at JPL for allowing the use of their facilities. He thanks Professor Fred Culick, Messrs. Warren Dowler, Winston Gin, and Leon Strand for their interest in these studies, and Messrs. Emilio Sovero, "Scott" Rasmussen, and David Daly for assistance at different stages of this work. He also thanks Mrs. Roberta Duffy for her quick and efficient typing.

List of Symbols

a	oxidizer particle size in microns or cm
a_{100}	the 100% wt. average point } fig. 13 shows
a_{50}	the 50% wt. average point } the details
A^*	nozzle throat area
c	specific heat
C^*	characteristic velocity of combustion gases
D^*	nozzle throat diameter
D	propellant diameter (= burner I. D.)
f	frequency (Hz)
L^*	chamber characteristic length ($\equiv V_c \div A^*$)
n	steady-state pressure index in ($r \propto P^n$)
$P, \bar{P}, P_c$	mean pressure in the chamber
$\lvert P' \rvert$	fluctuating pressure amplitude (peak to peak)
R	gas constant
r	instantaneous burning rate of propellant
$\bar{r}$	mean burning rate of propellant
T_f	flame temperature of combustion gases
t	time
u	gas flow velocity leaving the propellant surface
V_c	chamber free volume
κ^*	flame standoff distance above the burning propellant surface
κ	thermal diffusivity
ω	circular frequency ($\equiv 2\pi f$)
$( )_g$	gas phase
$( )_s$	condensed phase

References

1. Watermaier, L. A., et al. "An Experimental Investigation of Possible Aluminum Additive Contributions to Unstable Combustion in Solid Rocket Propellants," Report No. 1168, Ballistic Research Laboratories, Md. (1962).

2. Price, E. W. "Low-Frequency Combustion Instability of Solid Rocket Propellants," NOTS TP 3107 (1962).

3. Cieplucn, C. C. "Effect of Composition on Combustion of Solid Propellants During a Rapid Pressure Decrease," NASA TN D-1559 (1962).

4. Yount, R. A. and Angelus, T. A. "Chuffing and Nonacoustic Instability Phenomena in Solid Propellant Rockets," AIAA Preprint No. 64-148 (1964).

5. Eisel, J. L., et al. "Preferred Frequency Oscillatory Combustion of Solid Propellants," AIAA J., 2, 7 (1964), pp. 1319-1323.

6. Oberg, C. L. and Huebner, A. L. "Effects of Aluminum on Solid-Propellant Combustion Instability," Rocketdyne Report R-6654 (July 1966).

7. Jensen, G. E. "A Stop-Start Study of Solid Propellants," NASA CR-66488 (Nov. 1967).

8. Beckstead, M. W. Non-Acoustic Propellant Combustion Instability," Ph. D. Thesis, University of Utah (June 1965).

9. Beckstead, M. W., et al. "Nonacoustic Instability of Composite Propellant Combustion," AIAA J., 4, 9 (1966), pp. 1622-1628.

10. Beckstead, M. W. "Low Frequency Instability: A Comparison of Theory and Experiment," Combustion and Flame, 12 (Oct. 1968), pp. 417-426.

11. "Combustion of Solid Propellants and Low Frequency Combustion Instability," NOTS TP 4244, U. S. Naval Ordnance Test Station, China Lake, Calif. (1967).

12. Beckstead, M. W. and Price, E. W. "Nonacoustic Combustor Instability," AIAA J., 5, 11 (1967), pp. 1989-1996.

13. "Combustion of Solid Propellants and Low Frequency Combustion Instability," NWC TP 4478, U. S. Naval Weapons Center, China Lake, Calif. (1968).

14. Boggs, T. L. and Beckstead, M. W. "Failure of Existing Theories to Correlate Experimental Nonacoustic Combustion Instability Data," AIAA J. 8, 4 (April 1970), pp. 626-631.

15. Strand, L. D. "Summary of a Study of Low-Pressure Combustion of Solid Propellants," JPL Technical Report 32-1242 (April 1968).

16. Coates, R. L., et al. "An Interpretation of L^* Combustion Instability in Terms of Acoustic Instability Theory," AIAA J., 5, 6, (June 1967), pp. 1097-1102.

17. Wong, T. L. "Non-Acoustic Combustion Instability of Composite Propellants," Scientific Report to Combustion Energetics Div., AFOSR. University of Utah, Dept. of Chem. Eng. (1972).

18. Kumar, R. N. and McNamara, R. P. "Some Experiments Related to L-Star Instability in Rocket Motors," Guggenheim Jet Propulsion Center, Calif. Inst. of Technology (Mar. 1973).

19. Kumar, R. N. and McNamara, R. P. "Some Experiments Related to L-Star Instability in Rocket Motors," AIAA Paper No. 73-1300 (1973).

20. Seghal, R. and Strand, L. D. "A Theory of Low-Frequency Combustion Instability in Solid Rocket Motors," AIAA J., 2, 4 (1964), pp. 696-702.

21. Oberg, C. L. "Combustion Instability: The Relationship Between Acoustic and Non-acoustic Instability," AIAA J., 6, 2 (1968), pp. 265-271.

22. Culick, F. E. C. "Some Non-Acoustic Instabilities in Rocket Motors are Acoustic," AIAA J., 6, 7 (1968), pp. 1421-1423.

23. T'ien, J. S., et al. "Theory of L-Star Combustion Instability with Temperature Oscillations," AIAA J., 8, 1, (1970), pp. 120-126.

24. Law, C. K. and Williams, F. A. "Some Theoretical Aspects of the Influence of Solid Heterogeneity on L^* Instability," AIAA Paper No. 72-33 (1972).

25. Schöyer, H. F. R. "Report on Low-Frequency Oscillatory Combustion Experiments," Daniel and Florence Guggenheim Jet Propulsion Center, California Institute of Technology (1971).

26. Perry, E. H. "Investigations of the T-burner and Its Role in Combustion Instability Studies," Ph. D. Thesis, California Institute of Technology (Aug. 1972).

27. Loftus, H. J., et al. "Additives for Heat Flux Reduction," AIAA Paper No. 73-1289 (Nov. 1973).